Surface Micromachined MEMS Capacitors With Dual Cavity for Energy Harvesting

Jie Lin, Jianxiong Zhu, Yushan Chang, Zaichun Feng, and Mahmoud Almasri, *Senior Member, IEEE*

***Abstract*—A novel electrostatic MEMS capacitors array with dual capacitive cavities for energy harvesting from environmental vibration has been developed. This paper presents the new design, fabrication, modeling, and complete set of characterization of a MEMS capacitors array energy harvester with dual cavities, which achieves considerably higher energy generation than similar devices with a single capacitor. Rocking instability, that is, perturbations that may result in movable plates not in parallel to fixed plates, of the movable plate has been studied based upon comprehensive dynamic simulations using MATLAB. Resultant symmetric breaking causes drastic reduction on power generation. The devices have been successfully fabricated using surface micromachining technology and experimentally characterized. The resonance frequency is observed at 500 Hz. A maximum power of 2.5 μW across the load resistors is achieved under a high DC bias of 15 V and extremely intense excitation above 5 g. Detailed dynamic performance of the MEMS capacitors array energy harvester are presented in the paper. Experimental comparison between device with single capacitor and capacitors array are addressed. [2012-0367]**

***Index Terms*—MEMS capacitors array, electrostatic, energy harvester, Dual capacitive cavities.**

I. Introduction

MEMS micro-power source has drawn researchers' attentions worldwide as a promising solution to supply power for low energy consumption autonomous wireless sensor networks which have broad range of applications, such as structural health monitoring, predictive maintenance, biomedical implants, structure-embedded instrumentations, and automotive system [1]–[9]. One of most popular trends is to take advantage of ambient vibration for energy harvesting which is abundant and ubiquitously available on automobiles, airplanes, bridges, and so on. Reported microenergy harvesters in literatures for vibration-to-electric power conversion fall within three mechanism categories: electromagnetic [6], [10]–[13], piezoelectric [14]–[23], and electrostatic [36]–[42]. The electromagnetic transducer was commonly demonstrated as employing conventional permanent magnet moving through coils or coils integrated proof mass moving through the magnetic flux from a permanent magnet [6], [10], [11]. Many of applications using electromagnetic device were adapted in macroscale systems, because the achievements of gaining sufficient forces for low-frequency applications is still challenging in microdimensions [12], [13], and the integration of the bulky parts in such devices with complementary metal oxide semiconductor (CMOS) is costly. In addition, the micromachined electromagnetic harvesters tend to result in low output voltages making rectification difficult due to the limited number of coil turns [13]. The piezoelectric harvester utilizing piezoelectric material, such as PZT, in monolith or sputtered zinc oxide thin films into MEMS devices for vibration or motion energy harvesting were extensively investigated in literatures [14]–[17]. The mechanism exploits strains caused by mechanical vibrations in a piezoelectric material inducing a charge separation across the material therefore producing a voltage. Many of the reported piezoelectric transducers have overcome the limitation to low frequencies application [18], [19], and have achieved reasonable high voltages levels. However, the output impedance of the piezoelectric transducers is dominated by its capacitance, due to its small size cannot be turned out with a realistic inductance at the frequencies of interest [20]–[22]. The recent approaches combine the piezoelectric and electromagnetic mechanisms taking the advantage of magnetoelectric materials or magnetostricitve composites [23]–[25]. The advantages and disadvantages of each mechanism were comprehensively studied based upon existing prototypes of energy harvesters using different mechanisms [26], [27]; however, the conclusion of topgallant method is under debates, while the answer still cannot be addressed. Yeatman and his colleagues [28] performed extensive calculations and compared the normalized power of many inertial energy scavengers reported in literatures. They found that the power results do not show clear differences between the three transducer types in terms of normalized power [28]. We have chosen to work with electrostatic energy harvester. Although the achievable energy density is lower than that of piezoelectric and electromagnetic generators, it is CMOS compatible which allows the integration of power or communication electronic circuits and MEMS parts on one chip. This integration will lead to the production of low-cost arrays of microenergy sources.

Designs of many microdevices take advantage of the symmetry for better performance, immunity to noise, and simpler

Manuscript received December 8, 2012; revised March 21, 2013; accepted April 13, 2013. This work was supported by the National Science Foundation under Grant CMMI-0900727. Subject Editor R. Ghodssi.

J. Lin, Y.S. Chang, and M. Almasri are with the Department of Electrical and Computer Engineering, University of Missouri, Columbia, MO 65211 USA (e-mail: jlzm7@mail.missouri.edu).

J. X. Zhu and Z. C. Feng are with the Department of Mechanical and Aerospace Engineering, University of Missouri, Columbia, MO 65211 USA.

Color versions of one or more of the figures in this paper are available online at http://ieeexplore.ieee.org.

Digital Object Identifier 10.1109/JMEMS.2013.2262588

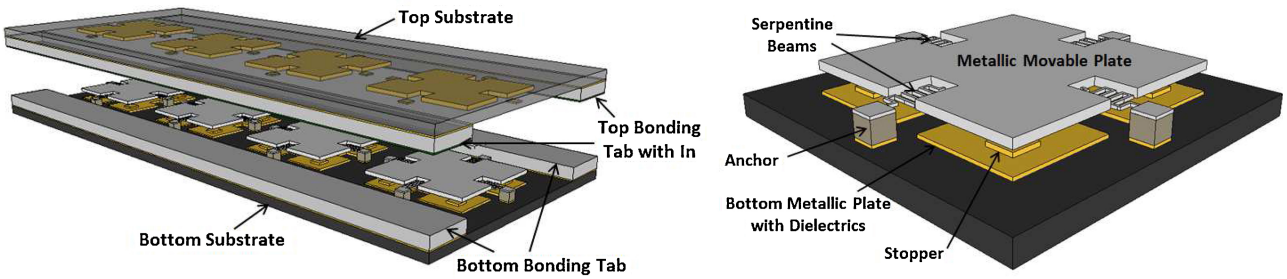

(a) (b)

Fig. 1. 3D Schematic of MEMS capacitors array energy harvester. (a) 3D view of the whole device, top substrate is risen up and made transparent for show. (b) Structure of movable plate.

analysis. When a symmetric structure is subjected to symmetric forcing, the symmetric response can become unstable leading to asymmetric responses. The occurrence of symmetry breaking bifurcation leads to complicated dynamic responses which often result in less desirable performances. There have been extensive dynamic studies on electrostatic MEMS power harvester using parallel plate structure which incorporates the nonlinear electrostatic, elastic, and squeeze film air damping in the model [29]–[31]. Most of researchers did not involve consideration of rotational motion of the movable plate which was normally treated as having only translational degree of freedom [33]. In this paper, we conduct numerical simulations to demonstrate the performances of our device with and without asymmetric dynamic responses resulting from the symmetry breaking.

In the last decade, a vast majority of electrostatic devices were designed and fabricated with structures, such as comb fingers or bulk micromachined proof mass suspended within a frame above the substrate for in-plane energy conversion [33]–[38]. To the best of our knowledge, no group has made attempts to fabricate MEMS parallel plate variable capacitors array for bi-directional energy harvesting for out of plane energy conversion. One disadvantage of electrostatic energy harvesters is that the devices always require a precharge voltage (supplied by external biasing DC) to operate. The precharging issue can be resolved by integrating an electret layer into the MEMS energy harvester for [5], [9], [39], [40]. Electret is the electrostatic analog of a magnet. It can be charged using corona discharging system [39], [41]–[44], and backlighted thyraton techniques [45]. Examples of electrets includes amorphous perfluorinated polymer (CYTOP) [43], polytetrafluoroethylene (PTFE) [46], and SiO_2/Si_3N_4 [41]. We are now performing researches on fabricating the electret materials with low aging decay which will be applied on our device in future process. In this paper, we will present a new design, modeling, dynamic simulation, and complete set of characterization on an improved type of dual cavity electrostatic MEMS energy harvester utilizing integrated capacitors array.

II. Design and Fabrication

A. Device Design

The MEMS capacitors array energy harvester is designed with four movable proof mass plates. Each is with an area and thickness of 2×2 mm^2 and 30 μm, respectively, suspended between two fixed plates on the top and bottom silicon substrates with two air gaps in between, forming two separate interactive vertical capacitors [see Fig. 1(a)]. When the capacitance increases for one cavity, it decreases for the other. This allows using both up and down directions to generate energy and thereby optimizing the efficiency of energy harvesting. The movable plates are supported by four serpentine springs with a thickness of 5 μm that are attached to the address lines on a silicon substrate only at the anchors' points which are made of electroplated nickel (Ni) [see Fig. 1(b)]. Five mechanical stoppers, made of gold, with height of 4 μm are electroplated on the fixed plates in order to prevent the pull-in behavior and modify the impact with the movable plate. SiO_2/Si_3N_4 thin layers were deposited and patterned to insulate the fixed plates with stoppers and enhance the dielectric property of the capacitive cavities. In addition, they can be used as an electret to trap charges at the interface between the two layers to create polarization voltage in capacitive cavities using Corona charging method in our future process [41].

The second air cavity is created by bonding a second silicon substrate onto the first one. The second substrate contains patterned fixed plates, SiO_2/Si_3N_4 dielectric layer, two strips of bonding tabs made of electroplated Ni, and thin layer of indium (In) for wafer bonding at low temperature and to provide electrical contacts to the electrodes. The strip bonding tabs on both substrates are aligned and bonded together when In layer is softened under relatively low temperature without damaging the integrity of whole device structure. The proof mass plates, serpentine suspension beams, anchors, and bonding tabs are all made of electroplated Ni which has been extensively studied as a mechanically durable material with controllable residual stress.

The MEMS capacitors energy harvester uses charge control strategy for power harvesting and operates as follows: the top and bottom capacitors are initially charged by a low-DC voltage source. When the plate moves down, capacitance of the bottom cavity increases and takes in charge from the low-DC -power source. Charging of bottom cavity stops when the plate reaches the lowest bottom position, then the plate tries to bounce back up so the gap of the bottom cavity increases and the gap of the top cavity decreases. Meanwhile, capacitance of the bottom cavity decreases and releases charge to

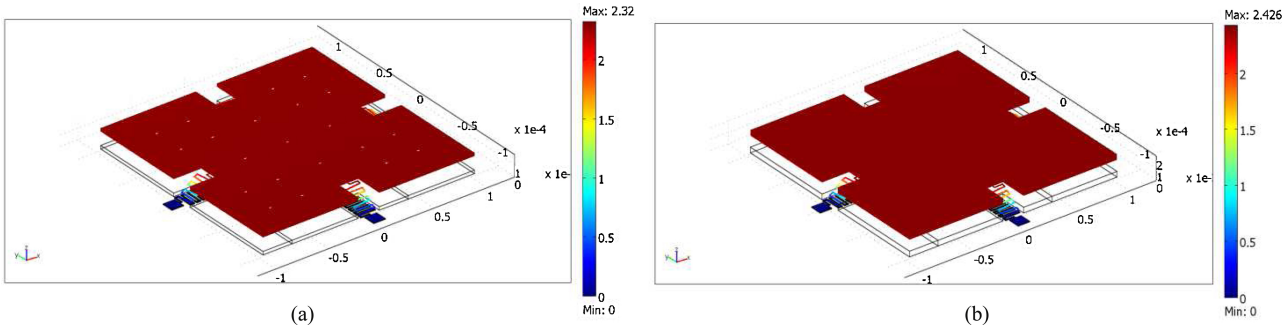

(a) (b)

Fig. 2. Finite element modeling of a vibrating movable plate with thickness of 30 and 50 μm, the resonance frequency of each device was found as follow. (a) 30 μm, 487 Hz. (b) 50 μm, 372 Hz.

corresponding load resistor, and capacitance of the top cavity starts increasing thereby taking charge from the low-DC power source. Discharging of top cavity to its load resistor starts as its capacitance decreases when plate reaches the highest top position and then moves back down again. Consequently, two out-of-phase AC signals are generated from two capacitive cavities as above sequence repeats when the movable plate is vibrating.

B. Finite Element Modeling

It has been investigated that a significant fraction of vibration energy is distributed within lower range of the frequency spectrum in many cases [27], typically below 500 Hz. Therefore, it is favorable to make vibrational energy harvester with a lower resonance frequency. To explore the resonance frequency of our design, the structure of the movable plate was modeled by COMSOL Multi-Physics finite element tool. Fig. 2(a) is a simulation of the movable plate having a thickness of 30 μm and the serpentine suspension beams having a width, thickness, and total length (four serpentine turns) of 15, 5, and 1485 μm, respectively. It is seem from the simulation that the plate vibrates uniformly without any distortion or warping. The resonance frequency was reported as 487 Hz. Another simulation was similarly implemented for the movable plate with a thickness of 50 μm, while other parameters were kept the same. It is proved by simulation that the corresponding resonance frequency can be lowered to 372 Hz by using heavier proof mass [Fig. 2(b)]. It should be noted that the above simulations were established without considering the impact of stoppers. Also, the experimental characterizations were performed on the device with serpentine suspension beams the same as the model in Fig. 2(a).

C. Device Fabrication Process

The MEMS capacitors array energy harvesters were fabricated on top of silicon substrates using surface micromachining technology as follows. i) 3-μm deep rectangular trenches were etched into a silicon wafer using reactive ion etch system (RIE) at locations corresponding to the capacitors' anchors and bonding tabs; ii) a SiO_2 insulation layer with a thickness of 1 μm was then thermally grown on the patterned wafer; iii) Cr and Au thin layers were sputter deposited, and Au layer was lithographically patterned to form the fixed plates, trace lines, electrode contacts, and the seed layer at locations corresponding to anchors of the movable plates and bonding tabs; iv) five Au stoppers were electroplated for a height of 4 μm on each fixed plate using a thick photoresist layer as mold; v) SiO_2 and Si_3N_4 were then sputter deposited and patterned using lift-off process to insulate the fixed plates with stoppers, and to enhance the dielectric property of capacitive cavities [see Fig. 3(a)]; vi) a thick photoresist sacrificial layer was patterned with a thickness of 30 μm serving as a mold for electroplating Ni anchors of the movable plate and bonding tabs. After completion of Ni electroplating, the photoresist sacrificial layer was cured in oven with an optimized temperature to prevent cracking and wrinkling; vii) a second seed layer of Cr and Au was similarly sputter deposited [see Fig. 3(b)]; viii) a photoresist mold with layouts of proof mass plates and serpentine beams was fabricated on top of the seed layer. Ni was similarly electroplated inside of this photoresist mold for a thickness of 5 μm. The proof mass plate thickness was increased to 30 μm (the thickness of suspension beams was kept the same) by electroplating Ni in another photoresist mold with only features of proof mass plate [see Fig. 3(c)]; and ix) finally, the photoresist molds on top of the second seed layer were removed by carefully flushing with acetone, isopropanol, and DI water without attacking the sacrificial layer. The second seed layer was then etched away using Au and Cr etchants. The sacrificial layer was last released in hot photoresist stripper bath with ultrasonic agitation. The Cr layer on the bottom substrate serving as first seed layer was finally etched away [see Fig. 3(d)]. The top substrate was fabricated with only fixed plates with dielectrics, stoppers, and bonding tabs by the same microfabrication procedures explained above. It should be pointed out that a thin layer of In for bonding two substrates was electroplated for 1 μm on the bonding tabs of top substrate. Two wafers containing top and bottom substrates were diced into small dies, each containing one device. The bonding tabs on top and bottom substrates were then aligned under the microscope with top substrate placed on a hotplate. A strong bond was formed when In layer was soften under 200 °C [see Fig. 3(e)].

III. Dynamic Studies

In the real world, rocking instability is inevitable for parallel movable plate structure (perturbations that may result in plates

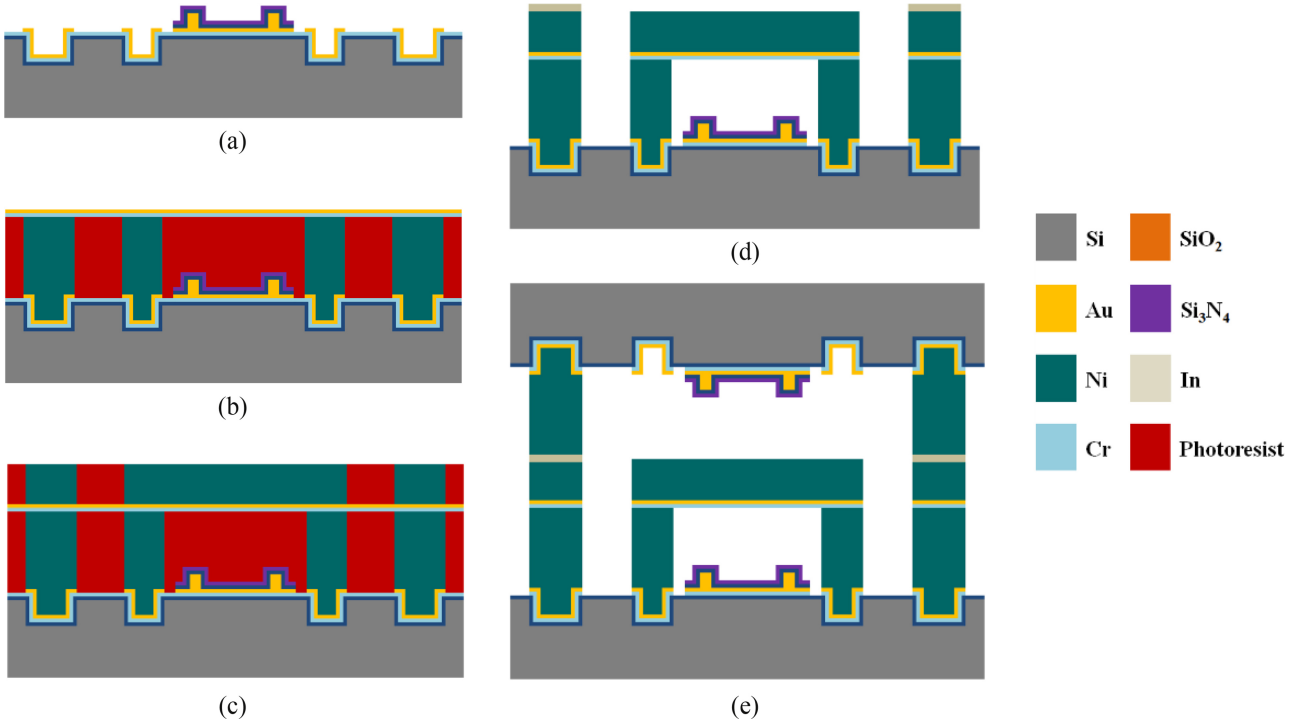

Fig. 3. Cross-section fabrication flow chart of MEMS capacitors array energy harvester with dual-cavity. (a) Pattern the fixed plates, trace lines, electrode contacts and seed layer, electroplate the stoppers, and deposit the dielectric layers. (b) Pattern the photoresist sacrificial layer, electroplate the anchors and bonding tabs, and deposit the second seed layer. (c) Electroplate the movable plate with suspension beams and the bonding tabs. (d) Release the photoresist layers, etch off the seed layers. (e) Bond the top substrate.

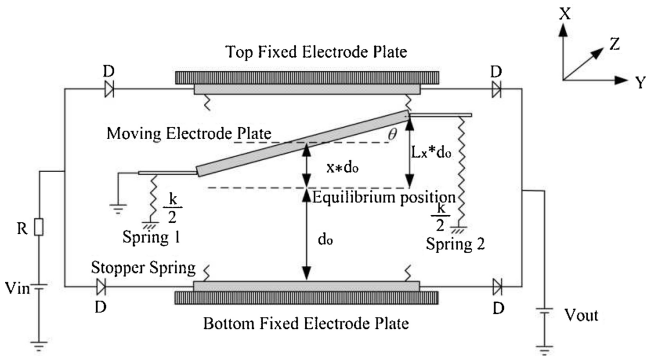

Fig. 4. Modeling schematic of electrostatic MEMS energy harvester with dual cavity involving rocking instability.

being no longer in parallel to each other). In other words, the movable plate behaves both vertical and rotational motion so that the tips of the movable plate are very likely to hit the stoppers or even fixed plates. A schematic of the typical model in Fig. 4 illustrates the device with onset of rocking instability. When the device is being charged, the voltage is varying as the movable plate is driven into motion by sinusoidal excitations. Low-DC voltage battery on the left of Fig. 4 is used to charge the device, and the raised voltage as the plate vibrates is released to the battery on the right. The value of V_{in} and V_{out} should be determined by specific application. They were chosen based upon general application for illustrative purpose in this modeling, $V_{\text{in}} = 5$ V and $V_{\text{out}} = 15$ V. Diodes are used to prevent the charge from flowing backwards. It should be pointed out that the diodes in this dynamic model are assumed to be ideal (leakage and parasitic capacitance are ignored). The R is a load resistor which is used to prevent the current from burning out the diodes. The movable plate is subjected to nonlinear electrostatic force F_{e}, linear suspension force, and sinusoidal excitation force F_{ex}. The stoppers with high stiffness are necessary to prevent the snap down of movable plate by overwhelming electrostatic force. Equation (1) was developed to simulate the elastic nonlinear force of the stoppers (stoppers' height equals 20% of capacitive gap) which may impact on the movable plate.

$$F_{\text{st}} = \begin{cases} \dfrac{-k_2 d_0(0.8 + L_x)}{1 + L_x} & -1 < x < -0.8 \\ & -0.8 < x < 0.8 \\ \dfrac{k_2 d_0(L_x - 0.8)}{1 - L_x} & 0.8 < x < 1 \end{cases};$$

$$L_x(\text{Left Tip}) = x - \frac{L\theta}{2d_0} \text{ and } L_x(\text{Right Tip}) = x + \frac{L\theta}{2d_0}, \quad (1)$$

where L_x is the dimensionless displacement of the left or right tip of the movable plate to the equilibrium position, k_2 is the spring constant of the stoppers, d_0 is the initial gap between the plates, L is the length of the movable plate, and θ is the deflection angle of the movable plate. The sinusoidal excitation force applied on the movable plate is simulated by (2).

$$F_{\text{ex}} = \alpha m(2\pi\gamma f)^2 \cos(2\pi\gamma f t), \quad (2)$$

where α is the imposed motion amplitude (higher value of α corresponds to heavier excitation), m is the mass of the movable plate, γ is the ratio of the excitation frequency to

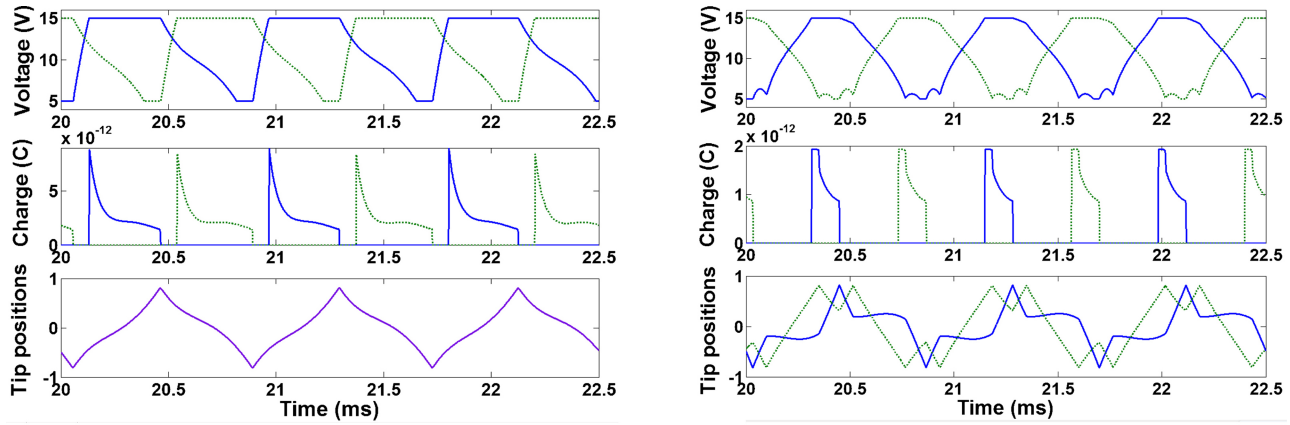

Fig. 5. Dynamic behaviors of electrostatic MEMS energy harvester with dual cavity under excitation amplitude of 20 μm, excitation frequency of 1200 Hz. (a) Without rocking. (b) With rocking.

the natural frequency, and f is the natural frequency. When the device vibrates with rocking, the deflection angle θ of movable plate will affect the nonlinear capacitance of top and bottom cavity. The capacitance given in (3) represents the capacitance of bottom cavity. The capacitance of top cavity can be obtained by reversing algebraic signs of x in (3). We calculated separately the electrostatic force and rotational moment of electrostatic force from each cavity. The electrostatic force and the rotational moment of electrostatic force are given by (4) and (6) when the device is in charging or discharging stage. When the device is in charge conservation stage, the electrostatic force and the rotational moment of electrostatic force are given by (5) and (7).

$$C(x,\theta)=\int_0^A \frac{\varepsilon dA}{g(x)}=\frac{\varepsilon W}{\theta}\mathrm{In}+\left(\frac{d_0+d_0x+\theta L/2}{d_0+d_0x-\theta L/2}\right)+\frac{\varepsilon W}{\theta}\mathrm{In}+\left(\frac{d_0-d_0x+\theta L/2}{d_0-d_0x-\theta L/2}\right) \tag{3}$$

$$F_e=-\frac{\partial U}{\partial x}=-\frac{\partial}{\partial x}\left(\frac{Q^2}{2C^2}C(x,\theta)\right)=\frac{V^2}{2}\frac{\partial}{\partial x}(C(x,\theta)) \tag{4}$$

$$F_e=-\frac{\partial U}{\partial x}=-\frac{\partial}{\partial x}\left(\frac{Q^2}{2C(x,\theta)}\right)=\frac{Q^2}{2}\frac{\partial}{\partial x}\left(\frac{1}{C(x,\theta)}\right) \tag{5}$$

$$M_e=-\frac{\partial U}{\partial x}=-\frac{\partial}{\partial x}\left(\frac{Q^2}{2C}\right)=\frac{V^2}{2}\frac{\partial}{\partial \theta}(C) \tag{6}$$

$$M_e=-\frac{\partial U}{\partial x}=-\frac{\partial}{\partial x}\left(\frac{Q^2}{2C^2}C\right)=-\frac{Q^2}{2}\frac{\partial}{\partial \theta}\frac{1}{C} \tag{7}$$

where ε is the permittivity of air, $g(x)$ is the varying gap, W and A is the width and area of the movable plate, U is the potential energy stored in capacitors, x is the differential displacement of the movable plate, and θ is differential angle of the movable plate. Equation (8) was developed to model the translational motion of the movable plate in vertical based on Newton's second law, and (9) models the rotational motion of the movable plate based on the law of rotation.

$$md_0\ddot{x}=-c_1d_0\dot{x}-kd_0x+F_{st}+F_e+F_{ex} \tag{8}$$

$$I_\theta\ddot{\theta}=-c_2\dot{\theta}-\frac{k}{8}L_2\theta+M_{st}+M_e,\ M_{st}=\frac{L}{2}F_{st} \tag{9}$$

where x is the dimensionless displacement, c_1 is the damping coefficient, k is the spring constant of suspension beams, c_2 is the damping coefficient for the rotational degree of freedom, $I\theta$ is the inertial constant of the movable plate, M_{st} is the rotational moment when the movable plate contacts with the stoppers, and M_e is the rotational moment of electrostatic force. We use (8) and (9) together to analyze the dynamic responses of the device when with and without the rocking instability. Numerical solutions of the equations of motion have led to the findings of very unusual responses. For example, Fig. 5 shows typical dynamic behaviors of the model in terms of voltage, charge, and tips' motion of the movable plate under excitation amplitude of 20 μm and excitation frequency of 1200 Hz with and without involving the rocking instability. The green curves on voltage versus time and charge versus time in Fig. 5 are presenting the changing of voltage and charge from the top cavity as the movable plate vibrates without [see Fig. 5(a)] and with [see Fig. 5(b)] rocking, and the blue curves are presenting the changing of voltage and charge from the bottom cavity. Much smaller magnitude of the changing of charge can be seen from the model with rocking in Fig. 5(b), which results in much less energy harvesting. The harvested power from the same model with and without the rocking instability over a broad range of frequencies and forcing amplitude are shown in Tables I and II. It should be pointed out that the rocking instability is initiated by involving a very small deflection angle on the movable plate in the initial condition, and the movable plate makes contact with the end stops in the simulations for most of these forcing parameters. We can see that the power generation is dramatically lowered by the onset of rocking instability in all conditions. However, it should be noticed that the harvested power in the dynamic studies is overestimated otherwise.

The two curves in the bottom panel of Fig. 5(b) represent the dimensionless positions of the two tips of the movable

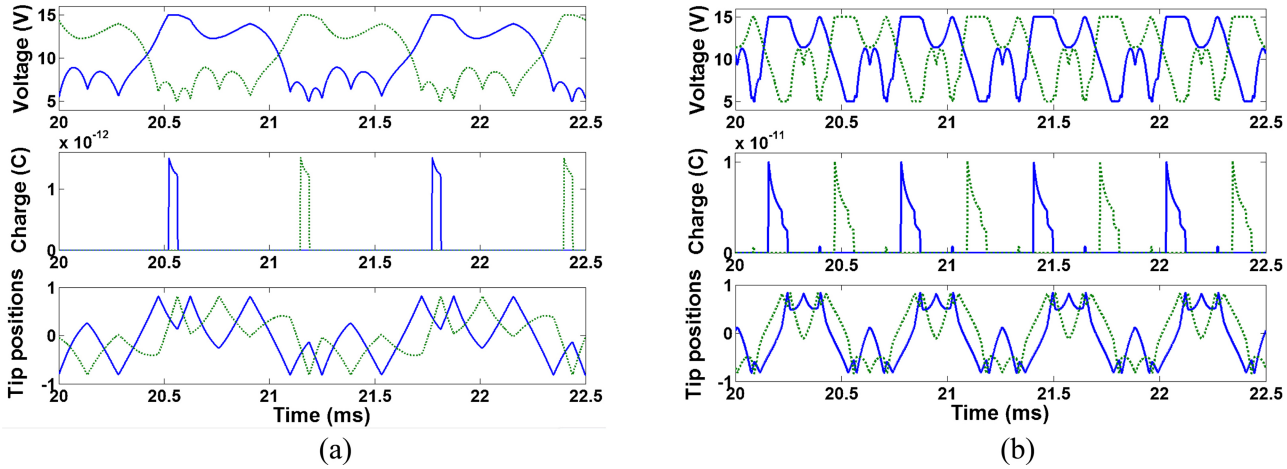

Fig. 6. Dynamic behaviors of electrostatic MEMS energy harvester with dual cavity with rocking. (a) Under 80 μm and 800 Hz excitation. (b) Under 80 μm and 1600 Hz excitation.

TABLE I
NUMERICAL RESULTS OF AVERAGE POWER (AVERAGE CURRENT × OUTPUT VOLTAGE) PRODUCED BY A DUAL-CAVITY MODEL WITHOUT ROCKING INSTABILITY

Excitation Amplitude (μm)	Average Power (μW) Produced By a Dual-Cavity Model Without Rocking Instability					
	Excitation Frequency = γ × Natural Frequency					
	γ=0.5	γ=1.0	γ=1.5	γ=2.0	γ=2.5	γ=3.0
80	10.54	27.85	49.74	68.68	93.66	121.9
60	10.35	23.92	37.94	58.86	74.71	94.74
40	0	21.75	42.64	58.52	64.7	93.39
20	0	21.02	32.98	46.03	59.97	76.15

TABLE II
NUMERICAL RESULTS OF AVERAGE POWER (AVERAGE CURRENT × OUTPUT VOLTAGE) PRODUCED BY A DUAL-CAVITY MODEL WITH ROCKING INSTABILITY

Excitation Amplitude (μm)	Average Power (μW) Produced By a Dual-Cavity Model With Rocking Instability					
	Excitation Frequency = γ × Natural Frequency					
	γ=0.5	γ=1.0	γ=1.5	γ=2.0	γ=2.5	γ=3.0
80	4.29	1.34	9.81	23.52	27.84	30.24
60	5.42	9.84	13.62	21.36	29.24	39.63
40	0	9.82	10	18.70	24.7	43.14
20	0	17.25	6.31	0.17	12.14	31.09

plate. The asymmetric dynamic motion of the movable plate can be seen when one tip of the plate impact the fixed plates twice, while the other tip only once. The curve of tip positions is marked in purple in Fig. 5(a), because the tips of plate are always at the same position since the model only involves translational motion in the vertical direction. More asymmetric dynamic behaviors under different excitation conditions are shown in Fig. 6. It is seen that plate responses are dominated by multiple impacts of the two tips with the fixed plate. In summary, when the motion of the movable plate is dominated by the separate impacts of two tips, the capacitance change of top and bottom cavity is much less than when the plates are in parallel. The harvested power is thus much reduced.

IV. RESULTS AND DISCUSSION

A. Fabrication Results

The MEMS capacitors array energy harvester with dual cavity has been fabricated using surface micromachining technology (see SEMs in Fig. 7). The movable plate was fabricated by Ni electroplating with proof mass's thickness of

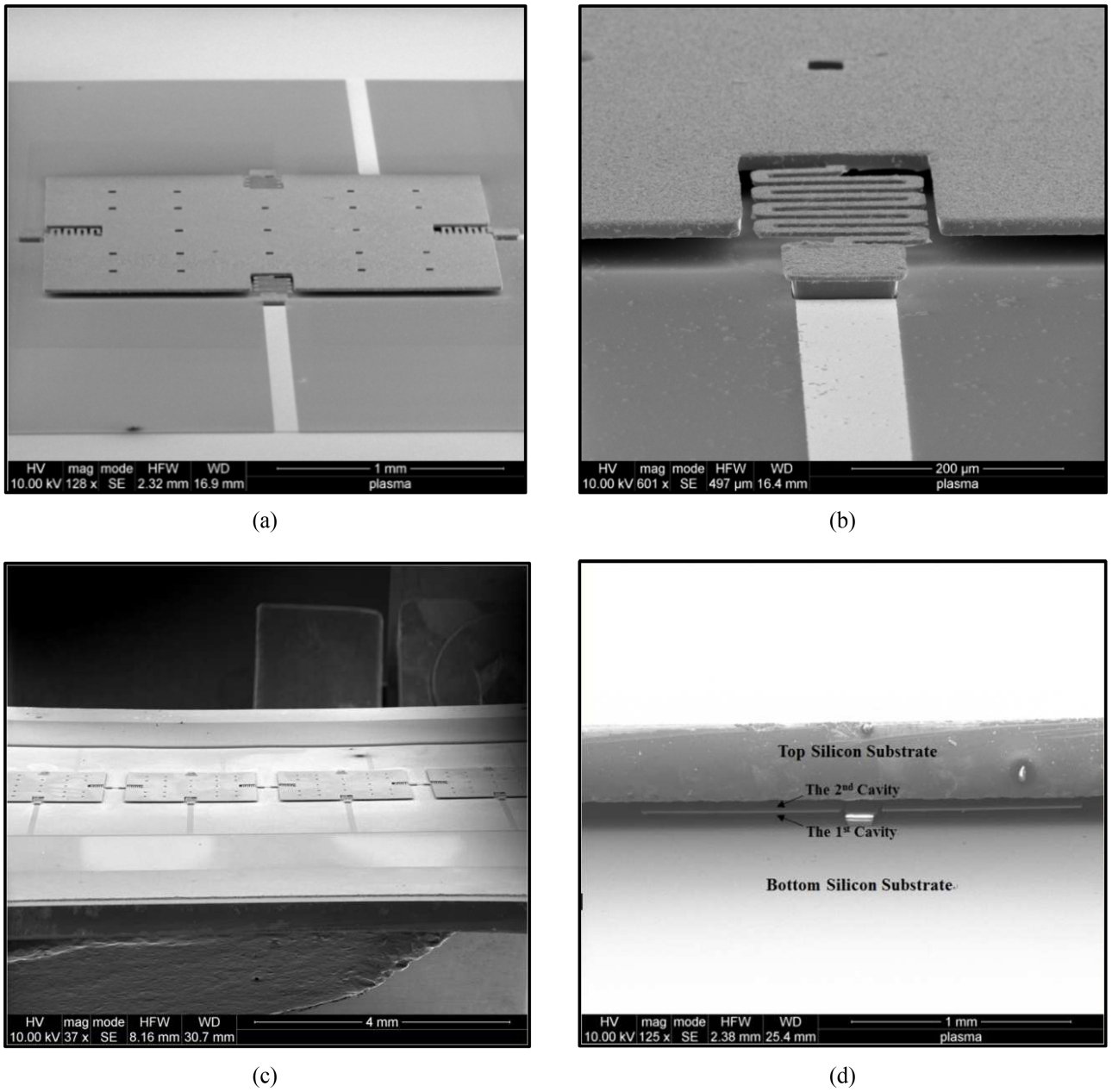

Fig. 7. SEMs of the MEMS capacitors array energy harvester with dual cavity before and after bonding the top cavity. (a) Single movable plate. (b) Magnified view of serpentine suspension beam. (c) Array capacitors before bonding the top cavity. (d) Bonded device with dual cavity.

30 μm [see Fig. 7(a)]. The serpentine suspension beams are made with a width, thickness, and total length (four serpentine turns) of 15, 5, and 1485 μm, respectively [see Fig. 7(b)]. The fabricated devices with two capacitive cavities are shown in Fig. 7(d) in which the air gap height of the top and bottom cavity is both 30 μm. The SEMs shows clearly that the device is suspended by four anchors and serpentine beams with sharp shapes. The movable plate was fabricated with a flat surface and square holes for device releasing as seen in Fig. 7(a). The top and bottom cavities with similar gap height are displayed clearly in Fig. 7(d).

B. Device Characterization and Discussion

The MEMS capacitors array energy harvester was experimentally characterized using a Printed Circuit Board test stage mounted on a shaker (Model Shop, TMS, K2007E type). The schematic of electrical characterization circuit and experimental setup are shown in Fig. 8. The device was firmly attached on the test stage. An analog accelerometer (Silicon Designs 1210L-050 type) was also mounted on the test stage beside the device and was used to measure the vibration conditions with respect to gravity (g). For an electrostatic energy harvester without built-in potential by electrets, it needs external bias DC to operate and generate energy. When the device was being DC biased with a low-DC source and driven into vibration by shaker, two AC signals generated across the two 5 MΩ load resistors and were measured through two unity amplifiers using a National Instrument DAQ (USB-6218 DAQ) and LabView interface in a PC. A programed circuit in Labview was automatically collecting the data from the

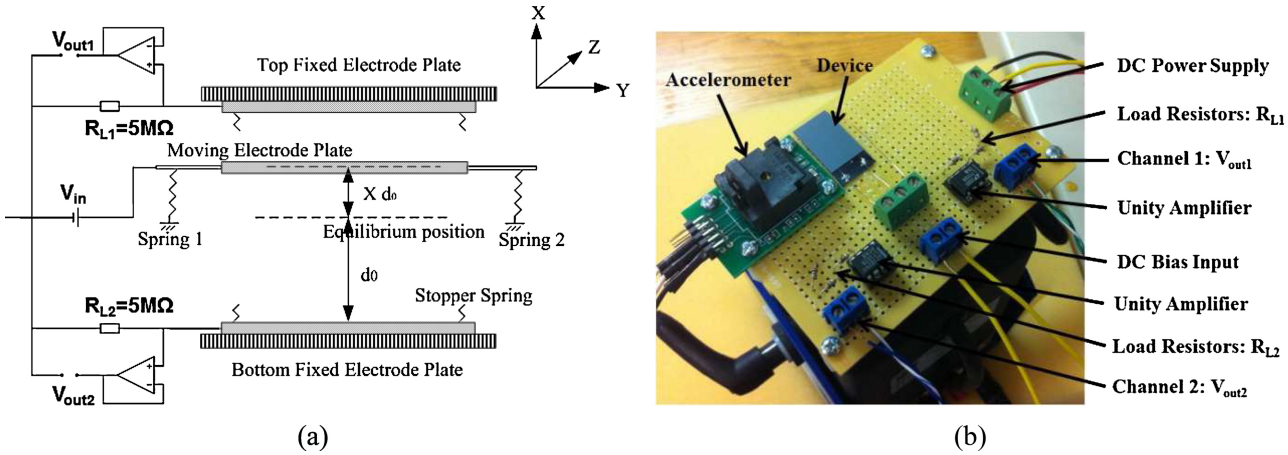

Fig. 8. Characterization circuit and setup. (a) Schematic of electrical characterization circuit. (b) Real experimental setup.

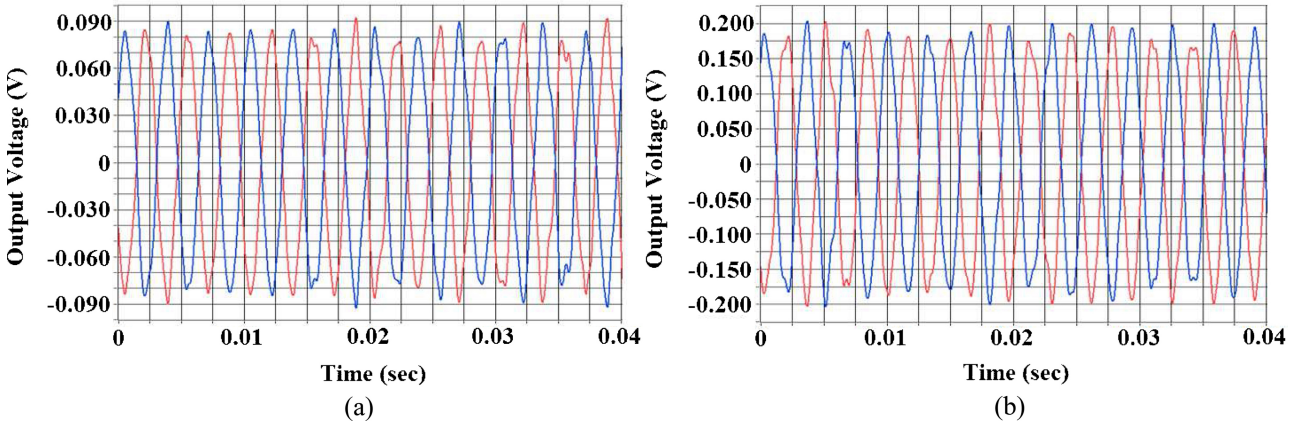

Fig. 9. Time domain plots of AC output voltage across the load resistors. (a) Device with single capacitor under 15 V DC bias, 300 Hz, and 1.026 g excitation. (b) Device with 1×4 capacitors array under 15 V DC bias, 300 Hz, and 1.020 g excitation.

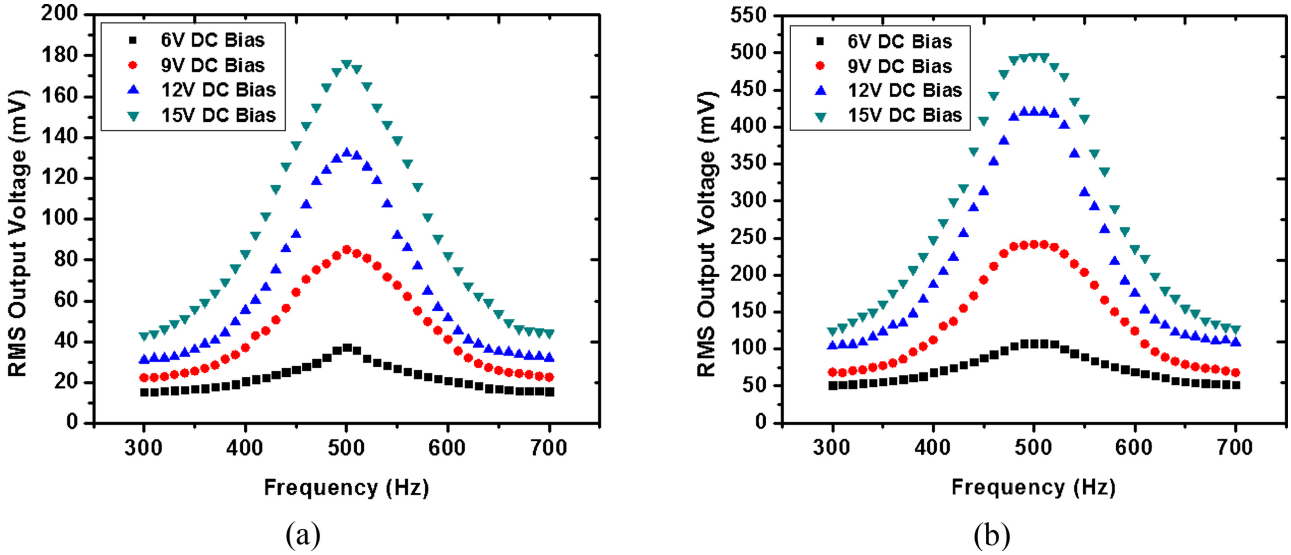

Fig. 10. RMS output voltage from bottom cavity of the devices as frequency sweeps. (a) Device with single capacitor under RMS excitation of 1.026 g. (b) Device with 1×4 capacitors array under RMS excitation of 1.020 g.

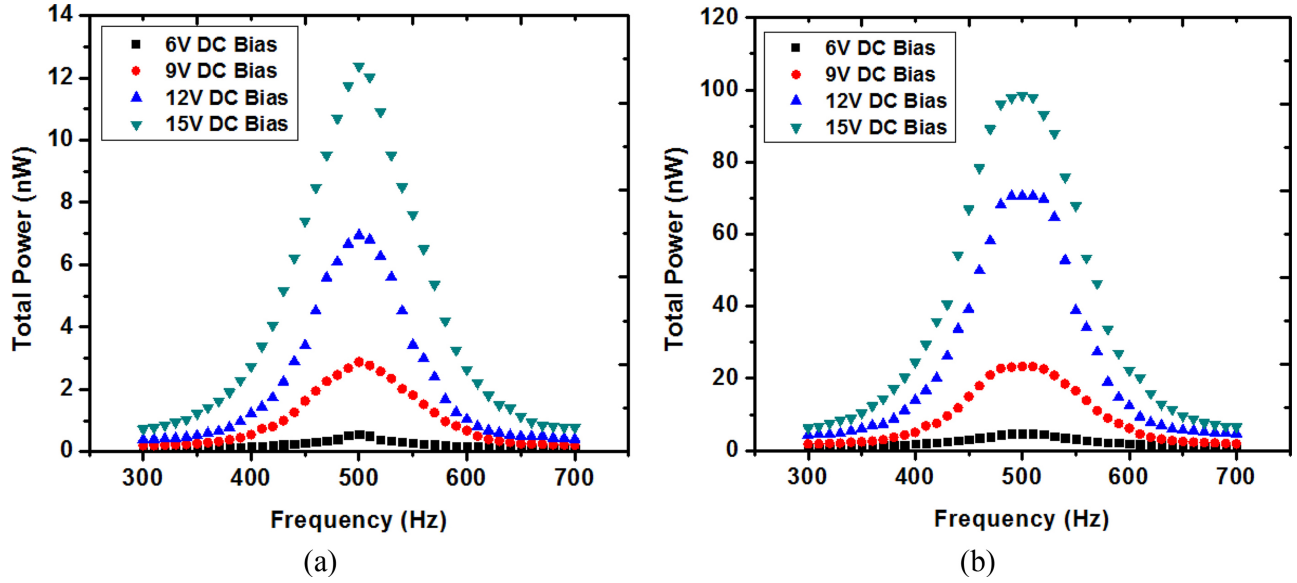

Fig. 11. Corresponding total power across two load resistors as frequency sweeps. (a) Device with single capacitor under RMS excitation of 1.026 g. (b) Device with 1×4 capacitors array under RMS excitation of 1.020 g.

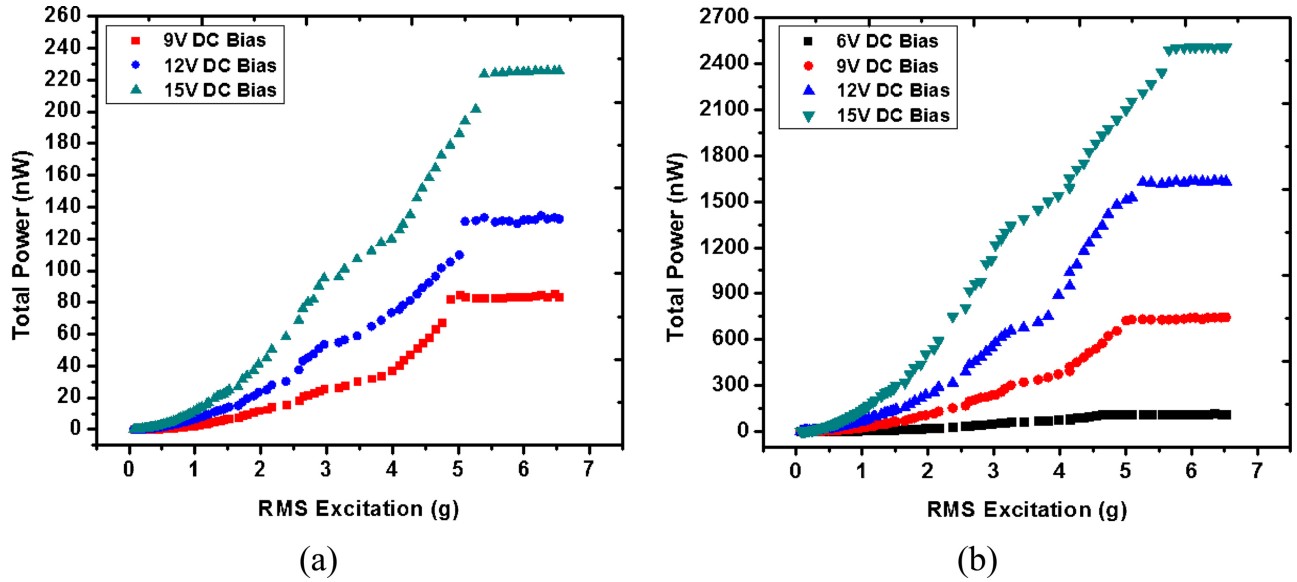

Fig. 12. Corresponding total power across two load resistors as excitation sweeps under a fixed frequency of 500 Hz. (a) Total power generated by single capacitor as function of excitation acceleration. (b) Total power generated by 1×4 capacitors array as function of excitation acceleration.

outputs of the unity amplifiers and the accelerometer. Each set of measurement lasted 30 s during which each output generated 375 sample data. The RMS voltage across each load resistor under different vibrations (with different frequency and acceleration) was calculated by averaging the 375 sample data from each set of measurement.

We have tested the devices with a single capacitor and 1×4 capacitor array. Fig. 9 shows two typical time domain plots of AC output voltage across the load resistors when the devices were being excited, in which two AC signals (marked as blue and red curves) corresponding to outputs from top and bottom cavity, respectively, are always out-of-phase. The devices were first characterized by sweeping the excitation frequency from 300 to 700 Hz with steps of 10 Hz under sinusoidal excitations with constant acceleration. The RMS output voltage under bias DC of 6, 9, 12, and 15 V from bottom cavity (V_{out2}) of each device were plotted as function of frequency (see Fig. 10). The resonance frequency was observed around 500 Hz for both devices. However, it is noticed that the device with capacitors array has broader bandwidth of resonance (around 480–520 Hz) than the device with single capacitor (sharply peaks at 500 Hz), which is ascribed to slightly different resonance response from each capacitor. We have selected the output voltage from bottom cavity (V_{out2}) to show the devices' responses, because the experimental results show that the outputs from top (V_{out1}) and

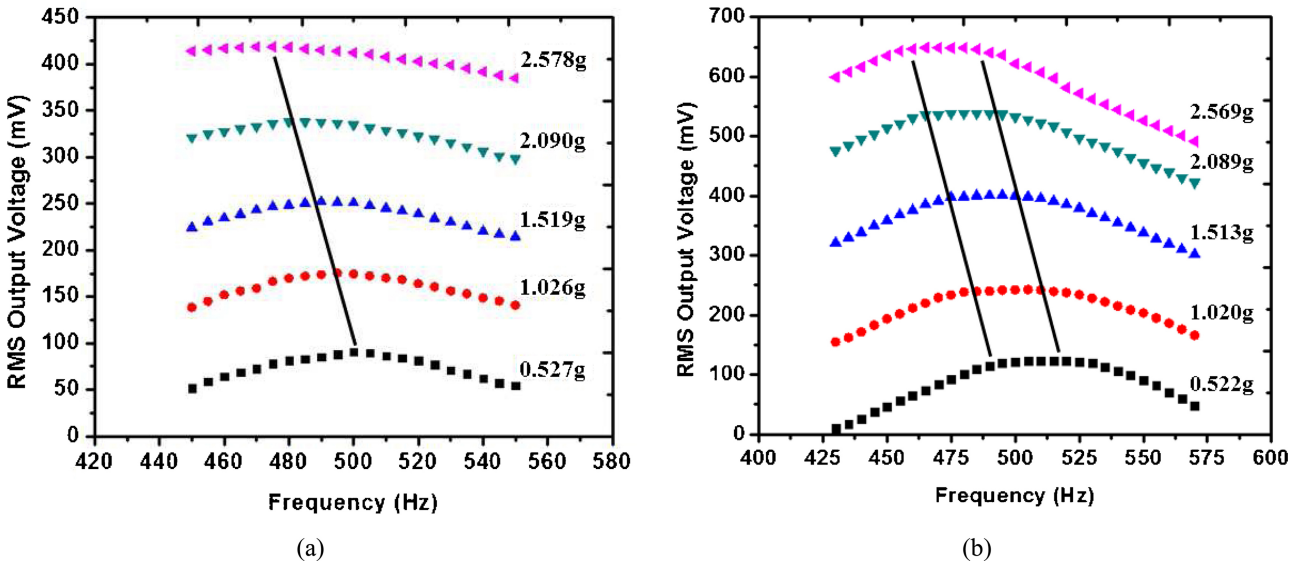

Fig. 13. RMS output voltage from bottom cavity of the devices as frequency sweeps under increasing excitation acceleration. (a) RMS output voltage from the single capacitor. (b) RMS output voltage from the 1×4 capacitors array.

bottom (V_{out2}) cavity are always nearly equivalent. In addition, because a clear resonant behavior was observed, we believe that the experimental forcing amplitude has not yet reached the value that we studied in the simulations and no contact between the movable plate and the fixed plates has taken place. The corresponding total power across two load resistors were calculated and plotted as function of frequency in Fig. 11.

The devices were then characterized under a fixed excitation frequency of 500 Hz while sweeping the excitation strength. The total measured power from two load resistors were observed increasing as excitation acceleration was sweeping up, and, then finally, saturating in extreme high excitation level (see Fig. 12). The measured power across the load resistors from the single capacitor and the capacitors array achieved a maximum power around 220 nW and 2.5 μW, respectively, under a high-DC bias of 15 V, and extremely intense excitation above 5 g (see Fig. 12). According to comprehensive experimental results, we observed that the measured RMS voltage from capacitors array is 3.2 times in average of that from single capacitor under extensive excitation conditions, which indicates that the capability of charge generation from array is 3.2 times higher in average than single capacitor due to its higher variation of capacitance. Since energy harvesting from the device is directly proportional to the generation of charge flow, it can be addressed that the capacitors array is capable of producing 3.2 times in average the power of single capacitor.

In an oscillating system, squeeze film air damping can make significant effects on the moving amplitude of the oscillating part and the resonance frequency, especially for those MEMS oscillators with parallel plate structure [47], [48]. For our devices, we experimentally investigated the squeeze film air damping by sweeping the excitation frequency within a narrow band width around devices' resonance frequency, and meanwhile increasing the excitation acceleration. In Fig 13(a), the RMS output voltage from the bottom cavity of the device with single capacitor under different excitation accelerations was plotted as function of frequency, which was sweeping up from 450 to 550 Hz with steps of 5 Hz. It is observed that the resonance frequency decreases from approximately 500 to 470 Hz as the excitation acceleration increases from 0.5 to 2.5 g. The same experiment was implemented on the 1×4 capacitors array. The device was similarly excited as the frequency increased from 430 to 570 Hz under increasing excitation accelerations from 0.5 to 2.5 g. The resonance frequency was also observed decreasing as the excitation was gradually increased [see Fig. 13(b)]. The observed frequency shifting might be considered as an evident phenomenon reflecting the squeeze film air damping; however, the conjecture is drawn purely base upon experimental behaviors. We currently do not have a developed numerical program to evaluate the true effect of squeeze film air damping mathematically because our system is complicated nonlinear dynamics with perforated movable plate. Analytical analysis of squeeze film air damping for such MEMS device requires modified Reynolds equation involving the damping effect of gas flow through holes on the movable plate [49]. We will perform extensive testing and numerical calculation on the effect of squeeze film air damping. Comparison between numerical analysis and experimental results will be reported in future work.

V. Conclusion

In this study, we have designed and modeled the MEMS capacitors array energy harvester with dual capacitive cavities using MEMS CAD tool and COMSOL Multi-Physics finite element tool. The designed structure was confirmed with good mechanical durability and appropriate resonance frequency.

We developed numerical program that is able to simulate the dynamic motion of the movable plate and calculated the total harvested power for given vibration amplitude and frequencies when the rocking instability is involved. It has been reported that the resultant symmetric breaking will cause drastic reduction on power generation. Prototypes of the device have been successfully fabricated using MEMS surface micromachining technology. Extensive characterizations have been performed on both fabricated devices with single capacitor and capacitors array for comparison. Both kinds of the device were observed with resonance frequency around 500 Hz. However, the resonance frequency of the device with capacitors array has been reported with broader bandwidth due to slightly different resonance response from each capacitor because of fabrication nonuniformity. When we increased excitation acceleration, a maximum power of 2.5 μW across the load resistors was achieved from the MEMS capacitors array energy harvester under a high DC bias of 15 V and extremely intense excitation above 5 g, by comparison, the energy harvester with single capacitor was reported with 220 nW as the maximum. Experimental results showed that the RMS voltage from capacitors array is 3.2 times in average of that from single capacitor. Therefore, we are able to draw the conclusion that the MEMS capacitors array energy harvester is capable of generating considerably higher energy than the energy harvester with single capacitor. In addition, the effect of squeezed air damping was experimentally explored. More extensive characterization and numerical analysis on the effect of squeeze film air damping will be reported in a future paper.

REFERENCES

[1] J. F. M. Oudenhoven, R. J. M. Vullers, and R. Schaijk, "A review of the present situation and future developments of micro-batteries for wireless autonomous sensor systems," *Int. J. Energy Res.*, vol. 36, no. 12, pp. 1139–1150, 2012.

[2] R. Torah, P. Glynne-Jones, M. Tudor, T. O'Donnell, S. Roy, and S. Beeby, "Self-powered autonomous wireless sensor node using vibration energy harvesting," *Meas. Sci. Technol.*, vol. 19, no. 12, p. 125202, 2008.

[3] N. G. Elvin, N. Lajnef, and A. A. Elvin, "Feasibility of structural monitoring with vibration powered sensors," *Smart Mater. Struct.*, vol. 15, no. 4, pp. 977–986, 2006.

[4] C. He, M. E. Kiziroglou, D. C. Yates, and E. M. Yeatman, "A MEMS self-powered sensor and RF transmission platform for WSN nodes," *IEEE Sensors J.*, vol. 11, no. 12, pp. 3437–3445, Dec. 2011.

[5] E. R. Westby and E. Halvorsen, "Design and modeling of a patterned-electret-based energy harvester for tire pressure monitoring systems," *IEEE/ASME Trans. Mechatronics*, vol. 17, no. 5, pp. 995–1005, Oct. 2012.

[6] F. Herrault, B. C. Yen, C. H. Ji, Z. S. Spakovszky, J. H. Lang, and M. G. Allen, "Fabrication and performance of silicon-embedded permanent-magnet microgenerators," *J. Microelectromech. Syst.*, vol. 19, no. 1, pp. 4–13, 2010.

[7] E. Jovanov and A. Milenkovic, "Body area networks for ubiquitous healthcare applications: Opportunities and challenges," *J. Med. Syst.*, vol. 35, no. 5, pp. 1245–1254, 2011.

[8] A. Shamim, M. Arsalan, L. Roy, M. Shams, and G. Tarr, "Wireless dosimeter: System-on-chip versus system-in-package for biomedical and space applications," *IEEE Trans. Circuits Syst. II*, vol. 55, no. 7, pp. 643–647, Jul. 2008.

[9] Y. Suzuki1, D. Miki, M. Edamoto, and M. Honzumi, "A MEMS electret generator with electrostatic levitation for vibration-driven energy-harvesting applications," *J. Micromech. Microeng.*, vol. 20, no. 10, pp. 104002-1–104002-8, 2010.

[10] S. P. Beeby, R. N. Torah, M. J. Tudor, P. Glynne-Jones, T. O'Donnell, C. R. Saha, and S. Roy, "A micro electromagnetic generator for vibration energy harvesting," *J. Micromech. Microeng.*, vol. 17, no. 7, pp. 1257–1265, 2007.

[11] C. Serre, A. Perez Rodriquez, N. Fondevilla, J. R. Morante, J. Montserrat, and J. Esteve, "Vibrational energy scavenging with Si technology electromagnetic inertial microgenerators," *Microsyst. Technol.*, vol. 13, no. 11–12, pp. 1655–1661, 2007.

[12] J. A. Paradiso and T. Starner, "Energy scavenging for mobile and wireless electronics," *IEEE Pervasive Comput.*, vol. 4, no. 1, pp. 18–27, Jan.–Mar. 2005.

[13] A. Khaligh, P. Zeng, and C. Zheng, "Kinetic energy harvesting using piezoelectric and electromagnetic technologies—State of the art," *IEEE Trans. Ind. Electron.*, vol. 57, no. 3, pp. 850–860, Mar. 2010.

[14] H. Liu, C. J. Tay, C. Quan, T. Kobayashi, and C. Lee, "Piezoelectric MEMS energy harvester for low-frequency vibrations with wideband operation range and steadily increased output power," *J. Microelectromech. Syst.*, vol. 20, no. 5, pp. 1131–1142, 2011.

[15] S. B. Kim, H. Park, S. H. Kim, H. C. Wikle, J. H. Park, and D. J. Kim, "Comparison of MEMS PZT cantilevers based on and modes for vibration energy harvesting," *J. Microelectromech. Syst.*, vol. 22, no. 1, pp. 26–33, 2013.

[16] E. K. Reilly, F. Burghardt, R. Fain, and P. Wright, "Powering a wireless sensor node with a vibration-driven piezoelectric energy harvester," *Smart Mater. Struct.*, vol. 20, no. 12, pp. 125006-1–125006-8, 2011.

[17] J. C. Park, S. Khym, and J. Y. Park, "Micro-fabricated lead zirconate titanate bent cantilever energy harvester with multi-dimensional operation," *Appl. Phys. Lett.*, vol. 102, no. 4, pp. 043901-1–043901-4, 2013.

[18] H. Liu, C. J. Tay, C. Quan, T. Kobayashi, and C. Lee, "Piezoelectric MEMS energy harvester for low-frequency vibrations with wideband operation range and steadily increased output power," *J. Microelectromech. Syst.*, vol. 20, no. 5, pp. 1131–1142, Oct. 2011.

[19] A. Massaro, S. De Guido, I. Ingrosso, R. Cingolani, M. De Vittorio, M. Cori, A. Bertacchini, L. Larcher, and A. Passaseo, "Freestanding piezoelectric rings for high efficiency energy harvesting at low frequency," *Appl. Phys. Lett.*, vol. 98, no. 5, pp. 053502-1–053502-3, 2011.

[20] S. P. Beeby, M. J. Tudor, and N. M. White, "Energy harvesting vibration sources for microsystems applications," *Meas. Sci. Technol.*, vol. 17, no. 12, pp. R175–R195, 2006.

[21] Y. C. Shu and I. C. Lien, "Efficiency of energy conversion for a piezoelectric power harvesting system," *J. Micromech. Microeng.*, vol. 16, no. 11, pp. 2429–2438, 2006.

[22] G. K. Ottman, H. F. Hofmann, and G. A. Lesieutre, "Optimized piezoelectric energy harvesting circuit using step-down converter in discontinuous conduction mode," *IEEE Trans. Power Electron.*, vol. 18, no. 2, pp. 696–703, Mar. 2003.

[23] T. Takahashi, M. Suzuki, T. Hirata, N. Matsushita, R. Yoneya, J. Onishi, T. Nishida, Y. Yoshikawa, and S. Aoyagi, "Electret energy harvesting based on fringe electrical field change inside trenched ferroelectric," in *Proc. IEEE MEMS*, Cancun, Mexico, Jan. 2011, pp. 1305–1308.

[24] C. S. Park, D. Avirovik, M. I. Bichurin, V. M. Petrov, and S. Priya, "Tunable magnetoelectric response of dimensionally gradient laminate composites," *Appl. Phys. Lett.*, vol. 100, no. 21, pp. 212901-1–212901-5, 2012.

[25] L. Chen, P. Li, Y. M. Wen, and D. Wang, "Magnetoelectric transducer employing piezoelectric ceramic/ferromagnetic alloy/high-permeability FeCuNbSiB composite," *IEEE Trans. Magn.*, vol. 47, no. 10, pp. 4437–4440, Oct. 2011.

[26] R. J. M. Vullers, R. van Schaijk, I. Doms, C. Van Hoof, and R. Mertens, "Micropower energy harvesting," *Solid-State Electron.*, vol. 53, no.7, pp. 684–693, 2009.

[27] S. Roundy, "On the effectiveness of vibration-based energy harvesting," *J. Intell. Mater. Syst.*, vol. 16, no. 10, pp. 809–823, 2005.

[28] P. D. Mitcheson, E. K. Reilly, T. Toh, P. K. Wright, and E. M. Yeatman, "Performance limits of the three MEMS inertial energy generator transduction types," *J. Micromech. Microeng.*, vol. 17, no. 9, pp. S211–S216, 2007.

[29] J. F. Rhoads, S. W. Shaw, and K. L. Turner, "Nonlinear dynamics and its applications in micro- and nanoresonators," *J. Dyn. Syst., Meas. Control Trans. ASME*, vol. 132, no. 3, pp. 034001-1–034001-14, 2010.

[30] E. K. Chan, K. Garikipati, and R. W. Dutton, "Characterization of contact electro-mechanics through capacitance-voltage measurements and simulations," *IEEE J. Microelectromech. Syst.*, vol. 8, no. 2, pp. 208–217, Jun. 1999.

[31] P. B. Chu and K. S. J. Pister, "Analysis of closed-loop control of parallel plate electrostatic microgrippers," in *Proc. IEEE Int. Conf. Robot. Autom.*, 1994, pp. 820–825.

[32] I. S. Joseph and E. B. Bernhard, "Dynamics and control of parallel-plate actuators beyond the electrostatic instability," in *Proc. IEEE Transducers*, Sendai, Japan, 1999, pp. 474–477.
[33] D. Hoffmann, B. Folkmer, and Y. Manoli, "Fabrication, characterization and modelling of electrostatic micro-generators," *J. Micromech. Microeng.*, vol. 19, no. 9, pp. 094001-1–094001-11, 2009.
[34] A. Modafe1, N. Ghalichechian1, A. Frey, J. H. Lang, and R. Ghodssi, "Microball-bearing-supported electrostatic micromachines with polymer dielectric films for electromechanical power conversion," *J. Micromech. Microeng.*, vol. 16, no. 9, pp. S182–S190, 2006.
[35] B. Andò, S. Baglio, G. L'Episcopo, and C. Trigona, "Investigation on mechanically bistable MEMS devices for energy harvesting from vibrations," *J. Microelectromech. Syst.*, vol. 21, no. 4, pp. 779–790, Aug. 2012.
[36] L. G. W. Tvedt, D. S. Nguyen, and E. Halvorsen, "Nonlinear behavior of an electrostatic energy harvester under wide- and narrow band excitation," *J. Microelectromech. Syst.*, vol. 19, no. 2, pp. 305–316, Apr. 2010.
[37] P. Basset, D. Galayko, A. M. Paracha, F. Marty, A. Dudka, and T. Bourouina, "A batch-fabricated and electret-free silicon electrostatic vibration energy harvester," *J. Micromech. Microeng.*, vol. 19, no. 11, pp. 115025-1–115025-12, 2009.
[38] W. Ma, R. Q. Zhu, L. Rufer, Y. Zohar, and M. Wong, "An integrated floating-electrode electric microgenerator," *J. Microelectromech. Syst.*, vol. 16, no. 1, pp. 29–37, Jan. 2007.
[39] M. Suzuki, T. Wada1, T. Takahashi, T. Matsushita, J. Onishi, T. Nishida, Y. Yoshikawa, and S. Aoyagi, "Fabrication of narrow comb-shaped electret by removing charge using excimer laser beam from charge-implanted CYTOP film for avoiding electrostatic repulsion problem," in *Proc. IEEE MEMS*, Paris, France, 2012, pp. 1229–1232.
[40] Z. H. Yang, J. Wang, and J. W. Zhang, "A high-performance micro electret power generator based on microball bearings," *J. Micromech. Microeng.*, vol. 21, no. 6, pp. 065001-1–065001-9, 2011.
[41] V. Leonov, P. Fiorini, and C. Van Hoof, "Stabilization of positive charge in SiO_2/Si_3N_4 electrets," *IEEE Trans. Dielectr. Electr. Insul.*, vol. 13, no. 5, pp. 1049–1056, Oct. 2006.
[42] Y. Wada, Y. Hamate, S. Nagasawa, and H. Kuwano, "Aging characteristics of electret used in a vibration-based electrostatic induction energy harvester," in *Proc. IEEE Transducers 2011*, Beijing, China, Jun. 2011. pp. 2626–2629.
[43] M. Kranz, M. G. Allen, and T. Hudson, "In situ wafer-level polarization of electret films in MEMS acoustic sensor arrays," *Sens. Actuators A, Phys.*, vol. 188, pp. 181–189, Dec. 2012.
[44] T. Onishi, T. Fujita, K. Fujii, K. Kanda, K. Maenaka, and K. Higuchi, "Selective electret charging method of SiO_2 film for energy harvesters by using biased electrode," in *Proc. World Autom. Congr.*, Puerto Vallarta, Mexico, 2012, pp. 1–5.
[45] T. Y. Hsu, W. H. Hsieh, Y. C. Tai, and K. Furutani, "A thin film teflon electret technology for microphone applications," in *Proc. Hilton Head Conf.*, 1996, pp. 235–238.
[46] Z. Yang, E. Halvorsen, and T. Dong, "Power generation from conductive droplet sliding on electret film," *Appl. Phys. Lett.* vol. 100, no. 21, pp. 213905-1–213905-4, 2012.
[47] L. Mol, L. A. Rocha, E. Cretu, and R. F. Wolffenbuttel, "Squeezed film damping measurements on a parallel-plate MEMS in the free molecule regime," *J. Micromech. Microeng.*, vol. 19, no. 7, pp. 2123–2129, 2009.
[48] M. H. Bao and H. Yang, "Squeeze film air damping in MEMS," *Sens. Actuators A, Phys.*, vol. 136, no. 1, pp. 3–27, 2007.
[49] M. H. Bao, H. Yang, Y. C. Sun, and P. J. French, "Modified Reynolds' equation and analytical analysis of squeeze-film air damping of perforated structures," *J. Micromech. Microeng.*, vol. 13, no. 6, pp. 795–800, 2003.

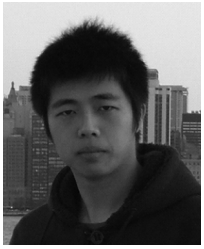

Jie Lin received the B.S. degree with double majors in physics and electronic engineering from the Pittsburg State University (PSU), Pittsburg, KS, USA in 2009. He is currently with the Microsystem Research Lab of Electrical and Computer Engineering Department at the University of Missouri (MU), Columbia, MO, USA, focusing on the design, modeling, fabrication, and characterization of electrostatic MEMS energy harvester. His current research interests include MEMS 3-D biosensors for foodborne pathogens detection and uncooled microbolometers for infrared detection.

Since August 2009, he has been a Ph.D. candidate in electrical and computer engineering at MU. He was with the Kansas Polymer Research Center at PSU as a Research Assistant, focusing on polymer engineering and characterization.

Jianxiong Zhu received the B.S. degree in electrical engineering and automation in 2006, and then he received the M.S. degree in safety science and engineering from the University of Science and Technology of China in 2010. He is currently a Ph.D. candidate in mechanical and aerospace engineering with the University of Missouri, Columbia, MO, USA, focusing on MEMS modeling and vibration analysis. His current research interests include the nonlinear dynamic analysis of the electrostatic MEMS power harvester, instability, oscillation, and bifurcation analysis of the various nonlinear vibration devices.

Yushan Chang received the B.S. degree in electrical engineering from the University of Missouri (MU), Columbia, MO, USA, in 2012, where she is currently an M.S. candidate in electrical engineering. Her current research interests include electrostatic MEMS energy harvesting.

Since 2011, she has been an Undergraduate Research Assistant in the Microsystem Research Lab of Electrical and Computer Engineering Department at MU.

Zaichun Feng is a Professor of mechanical and Aerospace Engineering at the University of Missouri, Columbia, MO, USA. His current research interests include the design and fabrication of micrgyroscopes, cell electrochemical sensors, microfluidic channels for cell sorting, polymer-derived ceramic heat flux sensor arrays, and capacitive power harvesters. He has conducted research on design, modeling, and fabrication of MEMS devices and microsensors funded by NSF, NIH, and U.S. Army PEO. He is a fellow of ASME.

Mahmoud Almasri (M'00-SM'12) received the B.Sc. and M.Sc. degrees in physics from Bogazici University, Istanbul, Turkey, in 1995 and 1997, respectively, and the Ph.D. degree in electrical engineering from Southern Methodist University, Dallas, TX, USA, in 2001. He is currently an Associate Professor with the Department of Electrical and Computer Engineering, University of Missouri, Columbia, MO, USA.

From 2001 to 2002, he was a Research Scientist with General Monitors, Lake Forest, CA, USA. From 2002 to 2003, he was with the College of Nanoscale Science and Engineering (formerly known as Albany NanoTech), State University of New York, Albany, NY, USA, as a Post-Doctoral Research Associate. From 2004 to 2005, he was with the Georgia Institute of Technology, Atlanta, GA, USA, as a Post-Doctoral Fellow, and then as a Research Scientist. His current research interests include three-dimensional biosensors, MEMS capacitors for power harvesting, Si-Ge-O infrared material and detectors, MEMS Coulter counters for studying time sensitive cells, and micropost arrays for measuring cell traction forces.